of white-radiation synchrotron X-ray topography, the second directed towards developing sophisticated 'beam conditioners' to extract highly collimated and monochromatic beams from the continuous-wavelength output of the synchrotron source. In both monochromatic and continuous-radiation experiments, the high intensity renders it more practicable than with conventional sources to apply electronic 'real-time' imaging systems (discussed in Sections 7.1.6 and 7.1.7, and Subsection 2.7.5.2).

At the experimental stations where synchrotron X-ray topography is performed, the distance a from the source (the tangent point on the electron orbit) is never less than some tens of metres, *e.g.* 40 m at the Deutsches Elektronen-Synchrotron, Hamburg (DESY), a maximum of 80 m at the Synchrotron Radiation Source, Daresbury (SRS), and 140 m at the European Synchrotron Radiation Facility (ESRF). The dimensions of the X-ray source (given by the cross section of the electron beam at the tangent point) vary widely between different installations (see Table 4.2.1.7), but the dimension in the plane of the electron orbit is usually several times that normal to it. If W_x and W_z are the corresponding full widths at half-maximum intensity of the source, then with the simple X-ray optics of a white-radiation topograph the geometrical resolution will be $W_x b/a$ and $W_z b/a$ in the orbit-plane (horizontal) and normal to the orbit-plane (vertical) directions, respectively, independent of the orientation of the plane of incidence of the Bragg reflection concerned. Representative dimensions might be $W_x = 2$ mm, $W_z = 0.5$ mm, and $a = 50$ m. With $b = 100$ mm, the horizontal and vertical resolutions of the topograph image would then be 4 and 1 μm, respectively, comparable with those on a conventional source, but with $b = 10$ mm only. Thus, even under synchrotron-source conditions, it is desirable that b should not exceed some centimetres in order to avoid geometrical factors causing a severer limitation of resolution (at least in one dimension) than other factors [such as photo-electron track lengths in the emulsion and point-by-point statistical fluctuations in absorbed photon dose (Lang, 1978)]. Since synchrotron X-rays are generated at all points along a curved electron trajectory, they spread out in a sheet parallel to the orbit plane. So there is in principle no limit to the specimen dimension in that plane that can be illuminated in a white-radiation topograph. However, increased background due to scattering from air and other sources imposes a practical limit of around 100 mm on the beam width. With electrons circulating in a planar orbit, the divergence of radiation normal to the orbit plane is strongly constricted, significant intensity being contained only within a fan of opening angle $\Omega \simeq mc^2/E$, *e.g.* $\Omega = 0.25$ mrad with electron energy $E = 2$ GeV, equivalent to a vertical distance $\sim$12 mm with $a = 50$ m. This does impose a significant restriction on the area of specimen that can be imaged in a transmission topograph unless recourse be had to beam expansion by an asymmetrically reflecting monochromator crystal.

For analysis of the three-dimensional configuration of defects within crystals, it is a useful feature of white-radiation transmission topography that different views of the specimen are presented simultaneously by the assemblage of Laue images, and that when studying reflection from a given Bragg plane there is freedom to vary the glancing angle upon it. When interpreting the diffraction contrast effects observed, the relative contributions of all the diffraction orders superimposed must be considered. However, after taking into account source spectral distribution, specimen structure factors, absorption losses and film efficiency, it is often found that a particular order of reflection is dominant in each Laue image (Tuomi, Naukkarinen & Rabe, 1974; Hart, 1975*a*). The variation of diffraction contrast with wavelength follows different trends for different types of defect (Lang, Makepeace, Moore & Machado, 1983), so the ability to vary the wavelength with which a given order of reflection is studied can help in identifying the type of defect.

If the orbiting electrons are confined to a plane, then the radiation emitted in that plane is completely linearly polarized with the **E** vector in that plane. It follows that diffraction with the plane of incidence normal to the orbit plane is in pure σ-polarization mode (polarization factor $P = 1$), and with plane of incidence parallel to the orbit plane in pure π-polarization mode ($P = |\cos 2\theta_B|$). The former, vertical plane of incidence is often chosen to avoid vanishing of reflections in the region of $2\theta_B = 90^\circ$. The ability to record patterns with either pure σ-mode or pure π-mode polarization is very helpful in the study of several dynamical diffraction phenomena. To facilitate switching of polarization mode, some diffractometers and cameras built for use with synchrotron sources are rotatable bodily about the incident-beam axis (Bonse & Fischer, 1981; Bowen, Clark, Davies, Nicholson, Roberts, Sherwood & Tanner, 1982; Bowen & Davies, 1983). From the diffraction-theoretical standpoint, it is the section topograph that provides the image of fundamental importance. High-resolution section-topograph patterns have been recorded with synchrotron radiation using a portable assembly combining crystal mount and narrow incident-beam slit. With the help of optical methods of alignment, this can be transferred between topograph cameras set up at a conventional source and at the synchrotron source (Lang, 1983).

The regularly pulsed time structure of synchrotron radiation can be exploited in stroboscopic X-ray topography. The wavefronts of travelling surface acoustic waves (SAW) on lithium niobate crystals have been imaged, and their perturbation by lattice defects disclosed (Whatmore, Goddard, Tanner & Clark, 1982; Cerva & Graeff, 1984, 1985). The latter workers made detailed studies of the relative contributions to the image made by orientation contrast and by 'wavefield deviation contrast' (*i.e.* contrast arising from deviation of the energy-flow vector in the elastically strained crystal).

2.7.4.2. *Incident-beam monochromatization*

In order to achieve extremely small beam divergences and wavelength pass bands ($\mathrm{d}\lambda/\lambda$), and, in particular, to suppress transmission of harmonic wavelengths, arrangements much more complicated than the double-crystal systems shown in Figs. 2.7.3.1 and 2.7.3.3 have been applied in synchrotron-radiation topography. The properties of monochromator crystals are discussed in Section 4.2.5. In synchrotron-radiation topographic applications, the majority of monochromators are constructed from perfect silicon, with occasional use of germanium. Damage-free surfaces of optical quality can be prepared in any orientation on silicon, and smooth-walled channels can be milled into silicon monoliths to produce multireflection devices. First, for simpler monochromatization systems, one possibility is to set up a monochromator crystal oriented for Bragg reflection with asymmetry $b \gg 1$ (*i.e.* giving $W_{\rm out}/W_{\rm in} \ll 1$) to produce a narrow monochromatic beam with which section topographs can be taken (Mai, Mardix & Lang, 1980). The standard $+-$ double-crystal topography arrangement is frequently used with synchrotron sources, the experimental procedure being as described in Section 2.7.3 and benefiting from the small divergence of the incident beam due to remoteness of the source. An example of a more refined angular probe is that obtainable by employing a pair of silicon crystals in $++$ setting to prepare the beam

Table 2.7.4.1. *Monolithic monochromator for plane-wave synchrotron-radiation topography*

Reflection 1	$\bar{3}33$
Reflection 2	$\bar{1}3\bar{1}$
Reflection 3	$1\bar{3}\bar{1}$
Output wavelength	0.12378 nm
Spectral pass band, $d\lambda/\lambda$	$\sim 7 \times 10^{-6}$
Angular divergence of exit beam	$\sim 1.4 \times 10^{-6}$
Size of exit beam	15×15 mm

incident on the specimen crystal, the three crystals together forming a $+ + -$ arrangement (Ishikawa, Kitano & Matsui, 1985). The first monochromator is oriented for asymmetric $11\bar{1}$ Bragg reflection, the second for highly asymmetric $55\bar{3}$ reflection ($W_{out}/W_{in} = 64$ at $\lambda = 0.12$ nm), resulting in a divergence of only 0.5×10^{-6} in the beam impinging on the specimen.

Multireflection systems, some of which were proposed by Du Mond (1937) but not at that time realizable, have become a practicality through the advent of perfect silicon and germanium. When multiple reflection occurs between the walls of a channel cut in a perfect crystal, the tails of the curve of angular dependence of reflection intensity can be greatly attenuated without much loss of reflectivity at the peak of the curve (Bonse & Hart, 1965*a*). Beaumont & Hart (1974) described combinations of such 'channel-cut' monochromators that were suitable for use with synchrotron sources. One combination, consisting of a pair of contra-rotating channel-cut crystals, with each channel acting as a pair of reflecting surfaces in symmetrical $+ -$ setting, has found much favour as a monochromatizing device producing neither angular deviation nor spatial displacement of the final beam, whatever the wavelength it is set to pass. The properties of monoliths with one or more channels and employing two or more asymmetric reflections in succession have been analysed by Kikuta & Kohra (1970), Kikuta (1971), and Matsushita, Kikuta & Kohra (1971).

Symmetric channel-cut monochromators in perfect undistorted crystals transmit harmonic reflections. Several approaches to the problem of harmonic elimination may be taken, such as one of the following procedures (or possibly more than one in combination).

(1) Using crystals of slightly different interplanar spacing (*e.g.* silicon and germanium) in the $+ -$ setting, which then becomes slightly dispersive (Bonse, Materlik & Schröder, 1976; Bauspiess, Bonse, Graeff & Rauch, 1977).

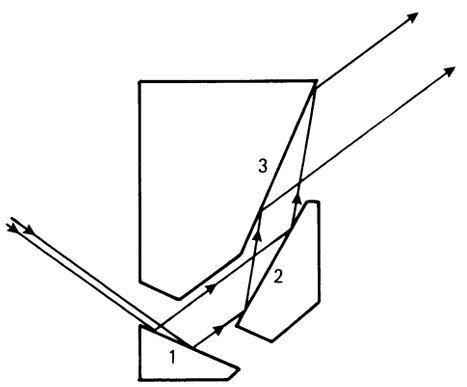

Fig. 2.7.4.1. Monolithic multiply reflecting monochromator for plane-wave topography.

(2) Laue case (transmission) followed by Bragg case (reflection), with deliberate slight misorientation between the diffracting elements (Materlik & Kostroun, 1980).

(3) Asymmetric reflection in non-parallel channel walls in a monolith (Hashizume, 1983).

(4) Misorientating a multiply reflecting channel, either one wall with respect to the opposite wall, or one length segment with respect to a following length segment (Hart & Rodrigues, 1978; Bonse, Olthoff-Münter & Rumpf, 1983; Hart, Rodrigues & Siddons, 1984).

For X-ray topographic applications, it is very desirable to have a spatially wide beam issuing from the multiply reflecting device. This is achieved, together with small angular divergence and spectral window, and without need of mechanical bending, in a monolith design by Hashizume, though it lacks wavelength tunability (Petroff, Sauvage, Riglet & Hashizume, 1980). The configuration of reflecting surfaces of this monolith is shown in Fig. 2.7.4.1. Reflection occurs in succession at surfaces 1, 2, and 3. The monochromator characteristics are listed in Table 2.7.4.1. The wavelength is very suitable in many topographic applications, and this design has proved to be an effective beam conditioner for use in synchrotron-radiation 'plane-wave' topography.

2.7.5. Some special techniques

2.7.5.1. *Moiré topography*

In X-ray optics, the same basic geometrical interpretation of moiré patterns applies as in light and electron optics. Suppose radiation passes successively through two periodic media, (1) and (2), whose reciprocal vectors are $\mathbf{h}_1$ and $\mathbf{h}_2$, so as to form a moiré pattern. Then, the reciprocal vector of the moiré fringes will be $\mathbf{H} = \mathbf{h}_1 - \mathbf{h}_2$. The magnitude, D, of the moiré fringe spacing is $|\mathbf{H}|^{-1}$ and may typically lie in the range 0.1 to 1 mm in the case of X-ray moiré patterns. Simple special cases are the 'rotation' moiré pattern in which $|\mathbf{h}_1| = |\mathbf{h}_2| = d^{-1}$, but $\mathbf{h}_1$ makes a small angle α with $\mathbf{h}_2$. Then, the spacing of the moiré fringes is d/α and the fringes run parallel to the bisector of the small angle α. The other special case is the 'compression' moiré pattern. Here, $\mathbf{h}_1$ and $\mathbf{h}_2$ are parallel but there is a small difference between their corresponding spacings, d_1 and d_2. The spacing D of compression moiré fringes is given by $D = d_1 d_2/(d_1 - d_2)$ and the fringes lie parallel to the grating rulings or Bragg planes in (1) and (2). X-ray moiré topographs achieve sensitivies of 10^{-7} to 10^{-8} in measuring orientation differences or relative differences in interplanar spacing. Moreover, if either periodic medium contains a lattice dislocation, Burgers vector $\mathbf{b}$, for which $\mathbf{b} \cdot \mathbf{h} \neq 0$, then a magnified image of the dislocation will appear in the moiré pattern, as one or more fringes terminating at the position of the dislocation, the number of terminating fringes being $\mathbf{b} \cdot \mathbf{h}$, which is necessarily integral (Hashimoto & Uyeda, 1957).

X-ray moiré topography has been performed with two quite different arrangements, the Bonse & Hart interferometer, and by superposition of separate crystals (Brádler & Lang, 1968). For accounts of the principles and applications of the interferometer, see, for example, Bonse & Hart (1965*b*, 1966), Hart (1968, 1975*b*), Bonse & Graeff (1977), Section 4.2.6 and §4.2.6.3.1. Fig. 2.7.5.1 shows the arrangement (Hart, 1968, 1972) for obtaining large-area moiré topographs by traversing the interferometer relative to a ribbon incident beam in similar fashion to taking a normal projection topograph (Fig. 2.7.2.2); P is the incident-beam slit, Q is a